Structure and superconductivity of the ternary intermetallics of $La_3Ni_4Si_4$, $La_3Ni_4Ge_4$, and $La_3Pd_4Si_4$

Structure and superconductivity of the ternary intermetallics of $La_3Ni_4Si_4$, $La_3Ni_4Ge_4$, and $La_3Pd_4Si_4$

H Fujii

Superconducting Materials Center, National Institute for Materials Science, 1-2-1 Sengen, Tsukuba, Ibaraki 305-0047, Japan

E-mail: fujii.hiroki@nims.go.jp

Abstract

Ternary intermetallics of $La_3Ni_4Si_4$, $La_3Ni_4Ge_4$, and $La_3Pd_4Si_4$ have been prepared by arc melting. These compounds take a body-centred lattice with an orthorhombic unit cell. The crystal structure of these compounds is $U_3Ni_4Si_4$ type with the space group *Immm*, consisting of the combination of structural units of AlB_2-type and $BaAl_4$-type layers, as observed for $La_3Pd_4Ge_4$. DC magnetization and electrical resistivity measurements indicate that $La_3Pd_4Si_4$ is a type II superconductor with a critical temperature (T_c) of 2.15 K. The lower critical field $H_{c1}(0)$ is estimated to be 28 Oe. On the other hand, the upper critical field $H_{c2}(0)$ estimated by the WHH theory is 2.2 kOe. The coherence length $\xi(0)$ of 38 nm and the penetration depth $\lambda(0)$ of 376 nm are derived. The other compounds $La_3Ni_4Si_4$ and $La_3Ni_4Ge_4$ do not show superconductivity above 1.8 K.

1. Introduction

Among ternary intermetallic compounds, $ThCr_2Si_2$-type intermetallics, RET_2X_2 (RE = rare earth, T = transition metal, X = Si and Ge), have been extensively studied, especially for the interest of the superconducting and magnetic properties. The structure of $ThCr_2Si_2$ is the ordered ternary derivative of the binary $BaAl_4$-type structure [1]. Although superconductivity is observed for some compounds, the critical temperature (T_c) is as low as 1 K, as reported for $LaPd_2Ge_2$ with a T_c of 1.12 K [2]. Many works were carried out for the discovery of new intermetallic superconductors with higher T_c values. Finally, quaternary intermetallic superconductors RET_2B_2C with $ThCr_2Si_2$-derivative structure showing high T_c values were discovered [3–6]. Among these compounds, YPd_2B_2C shows a T_c of 23 K, which is the highest among $ThCr_2Si_2$-type intermetallic compounds.

Apart from $ThCr_2Si_2$-type structure, another intermetallic superconductor, MgB_2, was discovered several years ago [7]. The MgB_2 shows a T_c as high as 39 K, which is the highest among intermetallic compounds. The structure of the MgB_2 is AlB_2-type structure, which

is composed of alternating of hexagonal layers of Al atoms and graphite-like honeycomb layers of B atoms. Many works have been done so far on the compounds with AlB_2-type structure after the discovery of MgB_2, and several superconductors with this structure have been reported [8, 9].

We have recently reported that $La_3Pd_4Ge_4$ is a type II superconductor with a T_c of 2.75 K [10]. The crystal structure of $La_3Pd_4Ge_4$ is $U_3Ni_4Si_4$ type with the space group of *Immm*, consisting of a combination of structural units of AlB_2-type and $BaAl_4$-type layers. In this paper, we report other analogue intermetallics of $La_3Ni_4Si_4$, $La_3Ni_4Ge_4$, and $La_3Pd_4Si_4$. Among them, the $La_3Pd_4Si_4$ is a type II superconductor with a T_c of 2.15 K. The other intermetallics do not show superconductivity above 1.8 K. We did not observe the formation of $La_3Pt_4X_4$ (X = Si and Ge) with $U_3Ni_4Si_4$-type structure.

2. Experimental details

Starting materials were La (chunk, 99.9% in purity), Ni (sheet, 99.99%), Pd (sheet, 99.99%), Pt (sheet, 99.99%), Si (granule, 99.999%), and Ge (granule, 99.999%). They were arc melted with a stoichiometric ratio of $La_3M_4X_4$ (M = Ni, Pd, and Pt; X = Si and Ge) under Ar gas atmosphere on a water-cooler copper hearth, except for the previously reported $La_3Pd_4Ge_4$ [10]. The melting was repeated several times with the button turned over between each melt. The weight loss was less than 1%. After melting, the obtained buttons wrapped in a Mo foil were annealed in an evacuated silica tube at temperatures between 1173 and 1373 K for one week. Some buttons of $La_3Pt_4X_4$ were annealed at temperatures between 1473 and 1673 K under a vacuum below 1×10^{-3} Pa for three days.

Phase identification was carried out for crushed samples by an x-ray diffraction (XRD) method with a JEOL JDX-3500 x-ray diffractometer. The XRD patterns were fitted using the Rietveld refinement program RIETAN 2000 [11]. Microstructural observation was carried out using a JEOL JSM-6301F scanning electron microscope (SEM) with an energy dispersive x-ray (EDX) spectrometer. Electron diffraction (ED) patterns and high-resolution electron microscope (HREM) images were recorded for crushed samples using a JEOL JEM-4000EX. The crushed samples were dispersed in CCl_4 and transferred to carbon coated copper grids. Image calculations were carried out using a MacTempas software program.

DC magnetization measurements were performed for bulk and crushed powder samples with a Quantum Design MPMS XL superconducting quantum interference device (SQUID) magnetometer. $M-H$ and $M-T$ curves were recorded at temperatures above 1.8 K in fields up to 1 kOe. The volume fraction of superconducting phase was estimated from the magnitude of zero-field-cooled (ZFC) magnetization in a field of 10 Oe in the $M-T$ measurements. The T_c was defined as the onset temperature where a diamagnetic signal was observed. Electrical resistivity measurements were carried out in the temperature range from 1.8 to 300 K by a standard DC four-probe method.

3. Results and discussion

3.1. Structural analyses

Most of the diffraction peaks in the XRD patterns were indexed on the basis of an orthorhombic unit cell with the same reflection condition of $h + k + l = 2n$ as observed for $La_3Pd_4Ge_4$ [10], except for the $La_3Pt_4X_4$ samples. This indicates that the lattice is body centred with a suggested space group of *Imm*2, *I*222, *I*$2_12_12_1$, or *Immm*. SEM-EDX analysis was performed on the polished cross section of the buttons of $La_3Ni_4Si_4$, $La_3Ni_4Ge_4$, and $La_3Pd_4Si_4$. The

Table 1. The lattice parameters and cell volume of La$_3$Ni$_4$Si$_4$, La$_3$Ni$_4$Ge$_4$, La$_3$Pd$_4$Si$_4$, and La$_3$Pd$_4$Ge$_4$ [10].

Compound	Lattice parameters (nm)			Cell volume (nm^3)
	a	b	c	
La$_3$Ni$_4$Si$_4$	0.413 08(5)	0.417 60(5)	2.3578(3)	0.406 73(8)
La$_3$Ni$_4$Ge$_4$	0.420 17(2)	0.421 67(3)	2.4031(1)	0.425 76(4)
La$_3$Pd$_4$Si$_4$	0.422 54(3)	0.428 71(3)	2.4551(2)	0.444 34(7)
La$_3$Pd$_4$Ge$_4$	0.422 00(3)	0.438 50(3)	2.5003(2)	0.462 67(5)

composition of the main phase in these samples was La:M:X = 3:4:4, indicating that the phase with the orthorhombic cell is La$_3$M$_4$X$_4$.

For M = Ni, the major impurity phase in these samples was identified as LaNi$_2$X$_2$ with the space group of $I4/mmm$, and some small XRD peaks could not be indexed on the basis of phases reported previously. On the other hand, for the La$_3$Pd$_4$Si$_4$ samples, the XRD peaks of impurity phases could not be assigned to LaPd$_2$Si$_2$. The impurity phases observed in the La$_3$Ni$_4$Si$_4$ and La$_3$Pd$_4$Si$_4$ samples are discussed below. It is noted that no trace of the orthorhombic phase was detected for the La$_3$Pt$_4$X$_4$ samples. The main phase observed in the La$_3$Pt$_4$X$_4$ samples was identified as LaPt$_2$X$_2$.

ED patterns taken along the various zone axes for La$_3$M$_4$X$_4$ suggest that the La$_3$M$_4$X$_4$ takes an orthorhombic unit cell. The lattice parameters of La$_3$M$_4$X$_4$ obtained from the ED patterns are in agreement with those obtained from the corresponding XRD patterns. Compared with the XRD analyses, no superstructure reflections were observed, and the reflection condition was the same, $h + k + l = 2n$, for all the samples.

The lattice parameters and the cell volume of La$_3$M$_4$X$_4$ obtained by XRD analyses are listed in table 1. The lattice parameters of La$_3$Ni$_4$Ge$_4$ are slightly smaller than the parameters reported previously for the single-crystalline sample, $a = 0.422\,34$ nm, $b = 0.422\,95$ nm, and $c = 2.4156$ nm [12]. The cell volume of La$_3$Ni$_4$Ge$_4$ is larger than that of La$_3$Ni$_4$Si$_4$, due to the large size of Ge. On the other hand, the lattice parameters of La$_3$Pd$_4$Si$_4$ are smaller than those of La$_3$Pd$_4$Ge$_4$ [10], due to the size difference between Si and Ge, as observed for La$_3$Ni$_4$Si$_4$ and La$_3$Ni$_4$Ge$_4$.

Rietveld pattern fitting for the XRD patterns was carried out for the compounds of La$_3$M$_4$Si$_4$ (M = Ni and Pd). The structure of La$_3$Ni$_4$Ge$_4$ has already been reported to be U$_3$Ni$_4$Si$_4$ type by XRD analyses using a single-crystalline sample [12]. The reflection conditions of XRD and ED patterns for La$_3$M$_4$Si$_4$ suggest four space groups, as mentioned above. The crystal structure of La$_3$M$_4$Si$_4$ was refined on the basis of the same U$_3$Ni$_4$Si$_4$-type structural model with the space group of $Immm$ as reported for La$_3$Ni$_4$Ge$_4$ and La$_3$Pd$_4$Ge$_4$. For M = Ni, the Rietveld refinements were carried out for the La$_3$Ni$_4$Si$_4$ and LaNi$_2$Si$_2$ phases simultaneously. For La$_3$Pd$_4$Si$_4$, the refinements were carried out only for this phase.

Table 2 lists the atomic parameters obtained by the Rietveld refinements for La$_3$Ni$_4$Si$_4$ and La$_3$Pd$_4$Si$_4$. Figures 1 and 2 illustrate the observed, the calculated, and the difference patterns for La$_3$Ni$_4$Si$_4$ and La$_3$Pd$_4$Si$_4$, respectively. The final R_{wp} factors are nearly the same for both compounds. They are 21.47 and 21.44% for La$_3$Ni$_4$Si$_4$ and La$_3$Pd$_4$Si$_4$, respectively. The isotropic thermal parameters B of all the atoms in La$_3$M$_4$Si$_4$ were fixed at 1.0 for the fitting, because the refinement of those B parameters caused not only smaller R_{wp} ($\approx$18–20%) but also $B < 0$. These relatively high R_{wp} factors do not suggest other structural models but come from the presence of impurity phases other than LaM$_2$Si$_2$. For M = Ni, the presence of LaNi$_2$Si$_2$ and the weight loss less than 1% after arc melting suggest the presence of small amounts of other

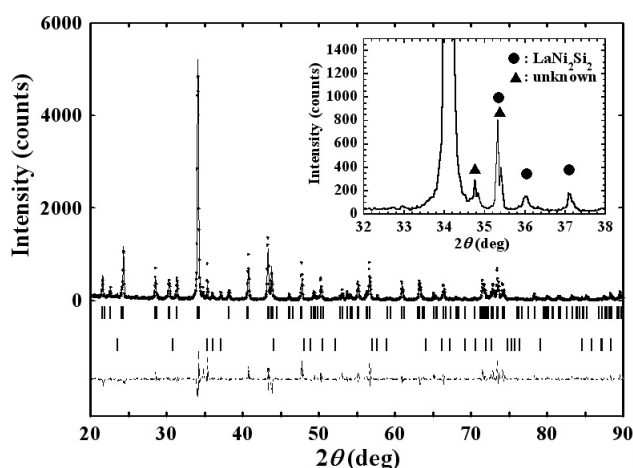**Figure 1.** Observed, calculated, and difference XRD data for $La_3Ni_4Si_4$. Plus marks (+) and the overlapped continuous line indicate the observed diffraction data and the calculated pattern, respectively. The refinement was carried out on the basis of a $U_3Ni_4Si_4$-type structural model with the space group of *Immm*. The background was fitted as a part of the refinement. The upper and lower vertical lines below the pattern denote the peak positions of $La_3Ni_4Si_4$ and $LaNi_2Si_2$, respectively. The difference between observed and calculated intensities is shown at the bottom in the same scale. The enlarged XRD pattern around $2\theta = 35°$ is shown in the inset. The XRD peaks of the $LaNi_2Si_2$ and unknown phases are marked by circles and triangles, respectively.

Table 2. The atomic parameters for $La_3M_4Si_4$ (M = Ni and Pd). g and B are the occupancy factor and the isotropic thermal parameter, respectively. Only the z parameters differ between $La_3Ni_4Si_4$ and $La_3Pd_4Si_4$. z(Ni) and z(Pd) denote the z parameters for $La_3Ni_4Si_4$ and $La_3Pd_4Si_4$, respectively.

Atom	Site	x	y	z(Ni)	z(Pd)	g	B (nm²)
La(1)	2a	0	0	0	0	1.0	0.01
La(2)	4j	0.5	0	0.3508(2)	0.3535(3)	1.0	0.01
M(1)	4j	0.5	0	0.0996(6)	0.0969(3)	1.0	0.01
M(2)	4i	0	0	0.2485(7)	0.2473(4)	1.0	0.01
Si(1)	4j	0.5	0	0.199(1)	0.199(1)	1.0	0.01
Si(2)	4i	0	0	0.447(1)	0.456(1)	1.0	0.01

impurity phases. Indeed, XRD peaks that cannot be assigned to either $LaNi_4Si_4$ or $LaNi_2Si_2$ were observed, as shown in the inset in figure 1. For $La_3Pd_4Si_4$, the peaks of $LaPd_2Si_2$ were not observed in the XRD pattern. However, the unknown impurity phases increase the R_{wp} factor, as shown in the inset in figure 2. The structural refinements on the basis of other space groups were not successful. Therefore, the $U_3Ni_4Si_4$-type structure with the space group of *Immm* is probably the most suitable for $La_3M_4Si_4$.

A [010] HREM image of $La_3Ni_4Si_4$ is shown in figure 3(a). Here the corresponding ED pattern and calculated image are together shown in the inset. The image calculations were carried out with the result of the Rietveld refinements listed in table 2. The calculated image along the [010] zone axis was obtained with $(\Delta f, t) = (-76$ nm, 1.7 nm). Here Δf and t denote defocus values and specimen thickness, respectively. Figure 3(b) shows a schematic view of the structure together with the enlarged calculated image along the [010] zone axis. In the experimental image, regular structure along the c-axis with the periodicity of 2.4 nm is clearly observed. Compared with the experimental and calculated images, the calculated
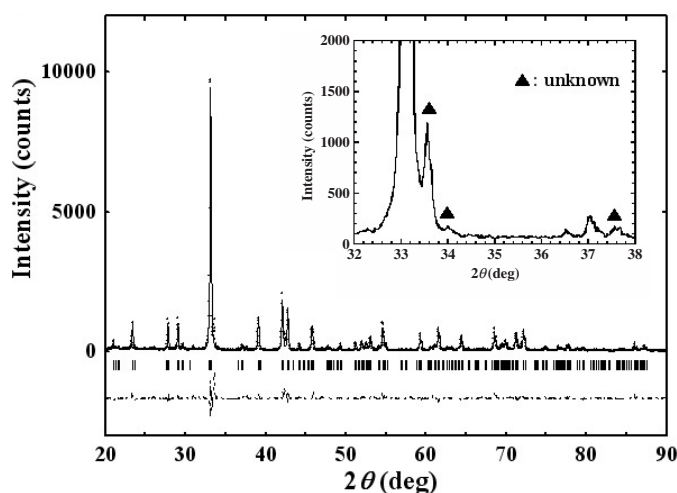
Figure 2. Observed, calculated, and difference XRD data for $La_3Pd_4Si_4$. Plus marks (+) and the overlapped continuous line indicate the observed diffraction data and the calculated pattern, respectively. The refinement was carried out on the basis of the $U_3Ni_4Si_4$-type structural model with the space group of *Immm*. The background was fitted as a part of the refinement. The vertical lines below the pattern denote the peak positions of La_3Pd_4Si. The difference between observed and calculated intensities is shown at the bottom in the same scale. The enlarged XRD pattern around $2\theta = 35°$ is shown in the inset. The XRD peaks of the unknown phases are marked by triangles.

image is in good agreement with the corresponding experimental image. With the results of the Rietveld refinements mentioned above, we conclude that the crystal structure of $La_3Ni_4Si_4$ is $U_3Ni_4Si_4$ type with the space group of *Immm*.

A [100] HREM image of $La_3Pd_4Si_4$ is shown in figure 4(a). Here the corresponding ED patterns and calculated images are also shown together in the inset. The image calculations were carried out with the result of the Rietveld refinements listed in table 2. The calculated image along the [100] zone axes was obtained with $(\Delta f, t) = (-74$ nm, 1.3 nm). Figure 4(b) shows a schematic view of the structure together with the enlarged calculated image along the [100] zone axes. In the experimental image, regular structure along the *c*-axis with the periodicity of 2.5 nm is clearly observed. Compared with the experimental and calculated images, the calculated image is in good agreement with the corresponding experimental image. With the results of the Rietveld refinements mentioned above, we conclude that the crystal structure of $La_3Pd_4Si_4$ is $U_3Ni_4Si_4$ type with the space group of *Immm*.

Figure 5 shows the crystal structure of $La_3M_4Si_4$ (M = Ni and Pd). This structure is composed of a combination of structural units of AlB_2-type and $BaAl_4$-type layers according to the relation $2La(M_{0.5}Si_{0.5})_2 + LaM_2Si_2 = La_3M_4Si_4$. The $U_3Ni_4Si_4$-type structure is observed for the other related germanides, such as $La_3Ni_4Ge_4$ and $La_3Pd_4Ge_4$, as mentioned above. Although the atomic radius of Pt is just slightly larger than that of Pd due to the lanthanide contraction, the $La_3Pt_4X_4$ phase with $U_3Ni_4Si_4$-type structure was not observed. For $U_3Ni_4Si_4$-type structure, Pd may be the upper limit from the viewpoint of size for $La_3M_4X_4$.

3.2. Physical properties

From XRD analyses, $La_3M_4X_4$ phase with $U_3Ni_4Si_4$-type structure was observed for $La_3Ni_4Si_4$, $La_3Ni_4Ge_4$, and $La_3Pd_4Si_4$. Although the structure of $La_3Ni_4Ge_4$ has already been reported using a single-crystalline sample, the physical properties have not been reported yet.
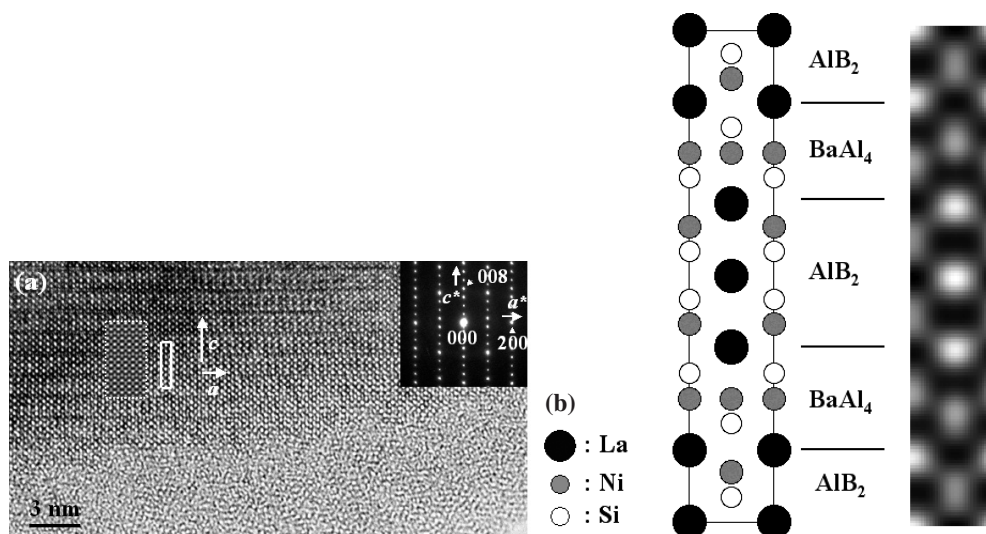
Figure 3. (a) An HREM image taken along the [010] zone axis for $La_3Ni_4Si_4$. The corresponding ED pattern and calculated image are shown in the inset. The unit cell and calculated image of $La_3Ni_4Si_4$ are indicated by solid and dashed lines, respectively, in the experimental image. Regular structure with the periodicity of 2.4 nm along the c-axis is observed. The calculated image was obtained with $(\Delta f, t) = (-76 \text{ nm}, 1.7 \text{ nm})$. Here Δf and t denote defocus values and specimen thickness, respectively. (b) A schematic view of the structure and the enlarged calculated image along the [010] zone axis for $La_3Ni_4Si_4$. The La atom is imaged as large white dots, whereas the Ni and Si atoms are merged as ellipsoidal grey dots.

Figure 6 shows the temperature dependence of DC magnetization curves for these compounds. The compounds of $La_3Ni_4Si_4$ and $La_3Ni_4Ge_4$ do not show a diamagnetic signal above 1.8 K, indicating that these compounds do not show superconductivity above this temperature. They do not show magnetic ordering, either. In contrast, $La_3Pd_4Si_4$ shows a large diamagnetic signal with the onset temperature of 2.15 K. At 1.8 K, the magnitude of the magnetic shielding signal after being corrected for demagnetization effects is approximately 80% of that estimated for perfect diamagnetism, while the magnitude of flux expulsion (Meissner effect) is about 6% of that estimated for perfect diamagnetism. The hysteresis observed between the signals in ZFC and field-cooled modes indicates that this compound is a type II superconductor. From the XRD analyses shown in figure 2, the $La_3Pd_4Si_4$ sample contains a small amount of impurity phases. However, the large volume fraction estimated from ZFC magnetization and the analogy to $La_3Pd_4Ge_4$ still suggest that the superconducting phase is $La_3Pd_4Si_4$.

Figure 7 shows the field dependence of magnetization curves $M(H)$ measured for the $La_3Pd_4Si_4$ bulk sample at various temperatures. These curves are also characteristic for type II superconductors. The apparent lower critical field (H_{c1}^*) of the $La_3Pd_4Si_4$ was determined by low field magnetization measurements. H_{c1}^* at various temperatures was taken as the point of deviation of $M(H)$ from the linear M–H behaviour observed at low magnetic fields. The true lower critical field (H_{c1}) was obtained from H_{c1}^* by applying the correction for the demagnetization factor. Fitting with the formula $H_{c1} = H_{c1}(0)[1 - (T/T_c)^2]$ results in $H_{c1}(0) = 28$ Oe, that is lower than that of $La_3Pd_4Ge_4$ ($H_{c1}(0) = 54$ Oe).

The upper critical field (H_{c2}) was estimated from both $M(H)$ and $M(T)$ curves. For the $M(H)$ curves, H_{c2} was determined from the point where the $M(H)$ curves reach the background. For the $M(T)$ curves, H_{c2} was estimated, taking account of the onset point of the
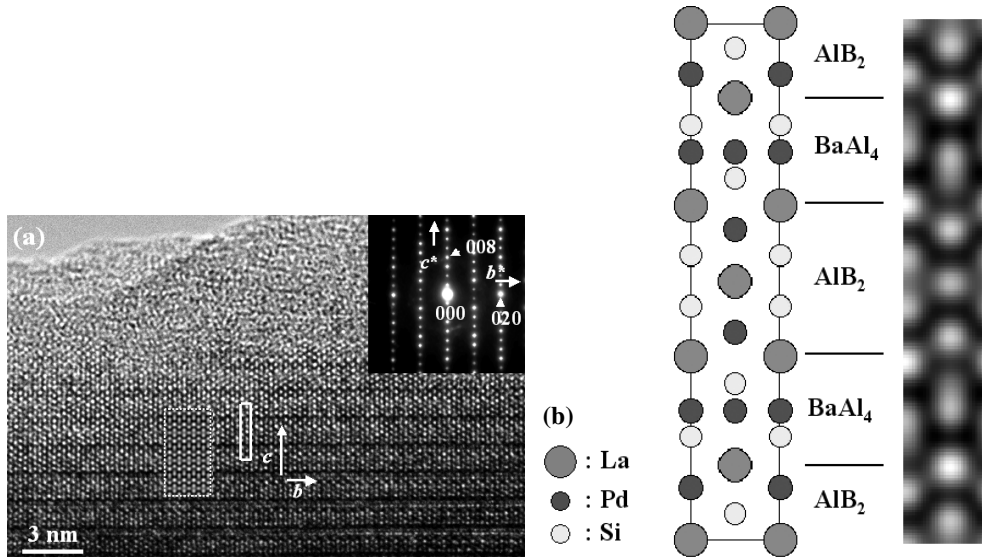
Figure 4. (a) An HREM image taken along the [100] zone axis for $La_3Pd_4Si_4$. The corresponding ED pattern and calculated image are shown in the inset. The unit cell and calculated image of $La_3Pd_4Si_4$ are indicated by solid and dashed lines, respectively, in the experimental image. Regular structure with the periodicity of 2.5 nm along the c-axis is observed. The calculated image was obtained with $(\Delta f, t) = (-74 \text{ nm}, 1.3 \text{ nm})$. Here Δf and t denote defocus values and specimen thickness, respectively. (b) A schematic view of the structure and the enlarged calculated image along the [100] zone axis for $La_3Pd_4Si_4$.

superconducting transition of the $M(T)$ curves. H_{c2} estimated from these curves as a function of temperature is shown in figure 8. The gradient $-dH_{c2}/dT$ is estimated to be 1.5 kOe K^{-1} for both $H_{c2}(T)$ curves. These values are comparable to that reported for $La_3Pd_4Ge_4$ with $-dH_{c2}/dT = 1.6$ kOe K^{-1} [10]. Linear extrapolation of the $H_{c2}(T)$ curves obtained from the $M(H)$ and $M(T)$ curves gives $H_{c2}(0)^{M-H} = 3.2$ kOe and $H_{c2}(0)^{M-T} = 3.3$ kOe, respectively. On the other hand, assuming the Werthamer–Hefland–Hohemberg (WHH) formula $H_{c2}(0)^{\text{WHH}} = -0.69T_c(dH_{c2}/dT)_{Tc}$ [13, 14], $H_{c2}(0)^{\text{WHH}}$ of 2.2 kOe is obtained from both $H_{c2}(T)$ curves. In the following calculations, $H_{c2}(0)^{\text{WHH}}$ is used for $H_{c2}(0)$.

With the formula $H_{c2} = \Phi_0/2\pi\xi^2$ (Φ_0 is the flux quantum), the coherence length $\xi(0)$ is estimated to be 38 nm, comparable to the value of 33 nm for $La_3Pd_4Ge_4$. This value is several times larger than those of borocarbide superconductors [5, 15] and MgB_2 [16]. From $H_{c2}(0)$ and $\xi(0)$, the penetration depth $\lambda(0)$ is calculated to be 376 nm, larger than that of $La_3Pd_4Ge_4$ at 248 nm, with the formula $H_{c1} = (\Phi_0/4\pi\lambda^2) \ln(\lambda/\xi)$. The Ginzburg–Landau parameter $\kappa(0)$ is 9.9, derived from the formula $\kappa(0) = \lambda(0)/\xi(0)$, and thermodynamic critical field $H_c(0)$ is 157 Oe with the formula of $H_c(0) = H_{c2}(0)/\sqrt{2}\kappa(0)$. Table 3 lists these measured and derived superconducting parameters.

The electrical resistivity ρ as a function of temperature for $La_3Ni_4Si_4$, $La_3Ni_4Ge_4$, and $La_3Pd_4Si_4$ is shown in figure 9. The detail of the region in the vicinity of T_c of $La_3Pd_4Si_4$ is shown in the inset. The resistivity decreases with decreasing temperature, showing metallic-type conductivity with a small negative curvature from 300 to 30 K for all the samples. Only $La_3Pd_4Si_4$ shows zero resistance at low temperature. The onset temperature of the transition is 2.20 K, and zero resistance is observed at 2.10 K. This is almost equal to the T_c value observed by the magnetization measurements shown in figure 6. For $La_3Pd_4Si_4$, the room temperature
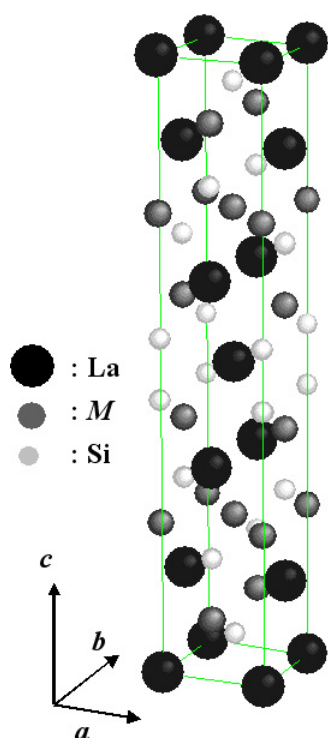
Figure 5. Crystal structure of $La_3M_4Si_4$ (M = Ni and Pd) with $U_3Ni_4Si_4$-type structure.
(This figure is in colour only in the electronic version)

Table 3. Measured and derived superconducting parameters for $La_3Pd_4Si_4$.

T_c (K)	2.15
$H_c(0)$ (Oe)	157
$H_{c1}(0)$ (Oe)	28
$H_{c2}(0)$ (kOe)	2.2
$\lambda(0)$ (nm)	376
$\xi(0)$ (nm)	38
$\kappa(0)$	9.9

resistivity, $\rho(300\text{ K})$, is approximately 60 $\mu\Omega$ cm, and the residual resistivity, $\rho(\text{res})$, just above T_c is 8 $\mu\Omega$ cm. The residual resistivity ratio (RRR) value is $\rho(300\text{ K})/\rho(\text{res}) = 7.5$. Other ternary superconducting silicides, such as $Sc_5Co_4Si_{10}$, show such small negative curvatures and comparable RRR values [17]. The RRR value of $La_3Pd_4Si_4$ is lower than that of the same $U_3Ni_4Si_4$-type $La_3Pd_4Ge_4$ ($\rho(300\text{ K})/\rho(\text{res}) = 270/11 = 24.5$) [10]. For $La_3Ni_4X_4$, $La_3Ni_4Ge_4$ is similar in behaviour to $La_3Pd_4Si_4$. The $\rho(300\text{ K})$ and $\rho(1.8\text{ K})$ are 64 and 12 $\mu\Omega$ cm, respectively. On the other hand, $La_3Ni_4Si_4$ shows high resistivities of 214 and 47 $\mu\Omega$ cm for $\rho(300\text{ K})$ and $\rho(1.8\text{ K})$, respectively. The relatively high resistivity at room temperature may be due to the high resistance at grain boundaries by the oxidation during heat treatment.

The temperature dependence of resistivity follows a power law function of temperature when the temperature of a metal is lowered. The ideal resistivity, $\rho_i(T)$, of a metal is given by
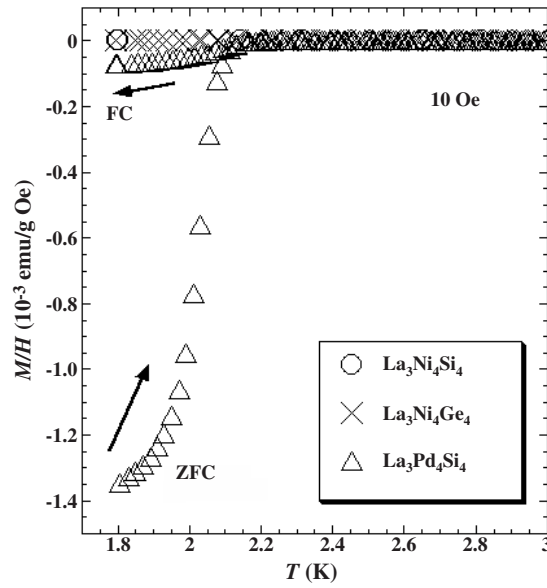
Figure 6. Temperature-dependent DC magnetization curves for La$_3$Ni$_4$Si$_4$, La$_3$Ni$_4$Ge$_4$, and La$_3$Pd$_4$Si$_4$. The data were recorded in ZFC and field-cooled modes. The applied field was 10 Oe.

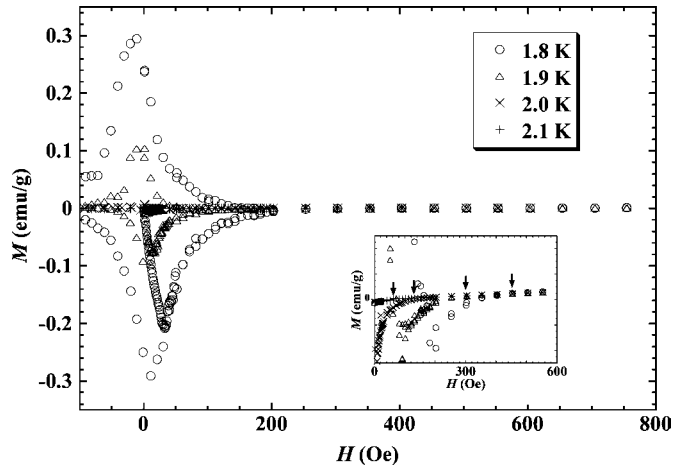**Figure 7.** Field dependence of magnetization curves $M(H)$ at various temperatures for La$_3$Pd$_4$Si$_4$. The details of the same curves in the background region are shown in the inset. The points where the $M(H)$ curves reach the background are indicated by arrows for each temperature.

the Bloch–Grüneissen formula:

$$\rho_i(T) = \rho_{\text{res}} + C \left(\frac{T}{\Theta_{\text{D}}} \right)^n \int_0^{\Theta D/T} \frac{x^n}{(1 - \exp^{-x})(\exp^x - 1)} \, dx,$$

where the first term ρ_{res} is the residual resistivity. The second term is due to scattering of electrons by phonons ($n = 5$) or to s–d-electron scattering ($n = 3$) where $x = \hbar v / kT$ and v is the phonon frequency. C is a numerical constant and Θ_{D} is the Debye temperature. In the low temperature region below 30 K, the $\rho(T)$ curves observed for these three compounds

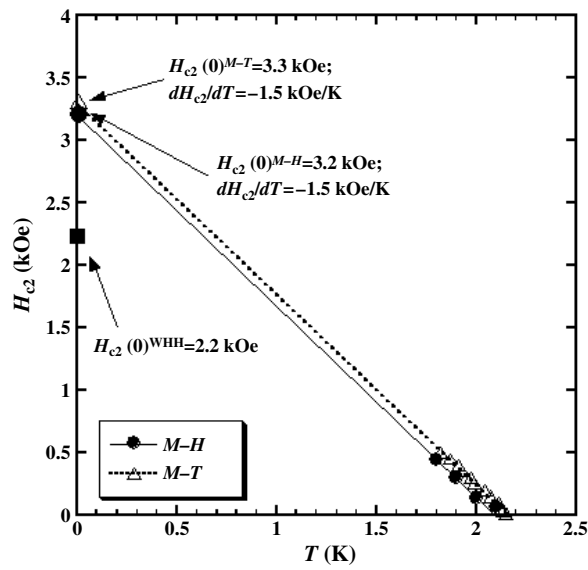**Figure 8.** Upper critical field H_{c2} obtained from $M(H)$ and $M(T)$ curves as a function of temperature for La$_3$Pd$_4$Si$_4$. The $H_{c2}(0)^{M-H}$ and $H_{c2}(0)^{M-T}$ denoted by a solid circle and a open triangle are estimated by linear extrapolation of the $H_{c2}(T)$ curves obtained from the $M(H)$ and $M(T)$ curves, respectively. The $H_{c2}(0)^{WHH}$ estimated by the WHH formula is denoted by a solid square.

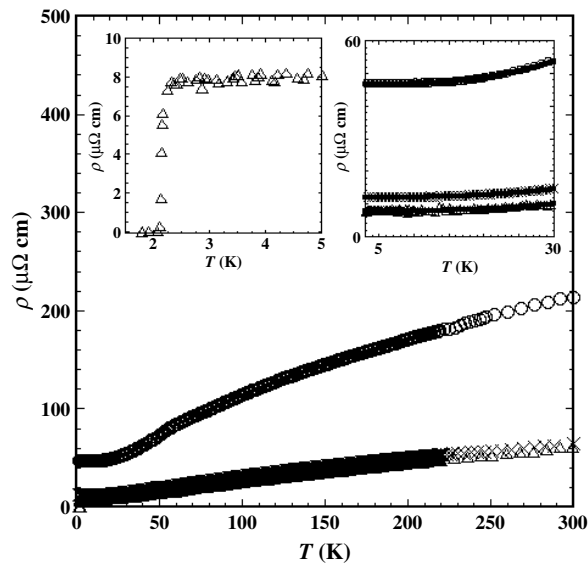**Figure 9.** Temperature-dependent electrical resistivity ρ for La$_3$Ni$_4$Si$_4$ (O), La$_3$Ni$_4$Ge$_4$ (×), and La$_3$Pd$_4$Si$_4$ (△). The insets show the detail of the region in the vicinity of T_c of La$_3$Pd$_4$Si$_4$ and a T^3 dependence of the $\rho(T)$ curves for these three samples in the low-temperature region (3 K < T < 30 K). Solid lines are fits to the Bloch–Grüneissen formula with $n = 3$.

were fitted with $n = 3$, as shown in the inset of figure 9, implying that the resistance is due to s–d-electron scattering.

The cell volume of La$_3$Pd$_4$Ge$_4$ is slightly larger than that of La$_3$Pd$_4$Si$_4$ by 4%. From the viewpoint of the bond length of La$_3$Pd$_4$X$_4$, the bond lengths of intralayer Pd(2)–Pd(2) and Pd–Si of La$_3$Pd$_4$Si$_4$ are smaller than those of intralayer Pd(2)–Pd(2) and Pd–Ge of La$_3$Pd$_4$Ge$_4$. Nevertheless, the T_c of La$_3$Pd$_4$Si$_4$ is lower than that of La$_3$Pd$_4$Ge$_4$. This is observed for the related BaAl$_4$-derivative ThCr$_2$Si$_2$-type compounds LaPd$_2$X$_2$ (X = Si and Ge), one of the constituting layers in La$_3$Pd$_4$X$_4$. The cell volumes of LaPd$_2$Si$_2$ and LaPd$_2$Ge$_2$ are 0.1807 and 0.1894 nm^3, respectively. The bond lengths of intralayer Pd–Pd and Pd–Si for LaPd$_2$Si$_2$ are shorter than those of intralayer Pd–Pd and Pd–Ge for LaPd$_2$Ge$_2$. Nevertheless, the T_c values of LaPd$_2$Si$_2$ and LaPd$_2$Ge$_2$ are 0.39 and 1.12 K, respectively [18, 2]. On the other hand, La$_3$Ni$_4$X$_4$ (X = Si and Ge) do not show superconductivity above 1.8 K. Band structure calculations are awaited to explain the variation of T_c in these La$_3$M$_4$X$_4$.

4. Conclusion

We have prepared ternary intermetallics of La$_3$Ni$_4$Si$_4$, La$_3$Ni$_4$Ge$_4$, and La$_3$Pd$_4$Si$_4$ by arc melting. The crystal structure of these compounds is U$_3$Ni$_4$Si$_4$ type with the space group of *Immm*, consisting of a combination of structural units of AlB$_2$-type and BaAl$_4$-type layers. DC magnetization and electrical resistivity measurements indicate that La$_3$Pd$_4$Si$_4$ is a type II superconductor with a T_c of 2.15 K. $H_{c1}(0)$ is estimated to be 28 Oe, and $H_{c2}(0)$ estimated by the WHH theory gives $H_{c2}(0)^{WHH} = 2.2$ kOe. The coherence length $\xi(0)$ of 38 nm and the penetration depth $\lambda(0)$ of 376 nm are derived. On the other hand, other compounds La$_3$Ni$_4$X$_4$ (X = Si and Ge) do not show either superconductivity or magnetic ordering above 1.8 K.

Acknowledgments

References

[1] Ban Z and Sikirica M 1965 *Acta Crystallogr.* **18** 594
[2] Hull G W, Wernick J H, Geballe T H, Waszczak J V and Bernardini J E 1981 *Phys. Rev.* B **24** 6715
[3] Cava R J, Takagi H, Batlogg B, Zandbergen H W, Krajewski J J, Peck W F Jr, van Dover R B, Felder R J, Siegrist T, Mizuhashi K, Lee J O, Eisaki H, Carter S A and Uchida S 1994 *Nature* **367** 146
[4] Cava R J, Takagi H, Zandbergen H W, Krajewski J J, Peck W F Jr, Siegrist T, Batlogg B, van Dover R B, Felder R J, Mizuhashi K, Lee J O, Eisaki H and Uchida S 1994 *Nature* **367** 252
[5] Cava R J, Batlogg B, Siegrist T, Krajewski J J, Peck W F Jr, Carter S, Felder R J, Takagi H and van Dover R B 1994 *Phys. Rev.* B **49** 12384
[6] Fujii H, Ikeda S, Kimura T, Arisawa S-i, Hirata K, Kumakura H, Kadowaki K and Togano K 1994 *Japan. J. Appl. Phys.* **33** L590
[7] Nagamatsu J, Nakagawa N, Muranaka T, Zenitani Y and Akimitsu J 2001 *Nature* **410** 63
[8] Cooper A S, Corenzwit E, Longinotti L D, Matthias B T and Zachariasen W H 1970 *Proc. Natl Acad. Sci.* **67** 313
[9] Imai M, Abe E, Ye J, Nishida K, Kimura T, Honma K, Abe H and Kitazawa H 2001 *Phys. Rev. Lett.* **87** 077003
[10] Fujii H, Mochiku T, Takeya H and Sato A 2005 *Phys. Rev.* B **72** 214520
[11] Izumi F and Ikeda T 2000 *Mater. Sci. Forum* **321–324** 198
[12] Bruskov V A, Bodak O I and Pecharskii V K 1986 *Inorg. Mater.* **22** 1384
[13] Helfand E and Werthamer W R 1966 *Phys. Rev.* **147** 288
[14] Werthamer N R, Helfand E and Hohemberg P C 1966 *Phys. Rev.* **147** 295
[15] Takagi H, Cava R J, Eisaki H, Lee J O, Mizuhashi K, Batlogg B, Uchida S, Krajewski J J and Peck W F Jr 1994 *Physica* C **228** 389
[16] Buzea C and Yamashita T 2001 *Supercond. Sci. Technol.* **14** R115
[17] Hausermann-Berg L S and Shelton R N 1987 *Phys. Rev.* B **35** 4673
[18] Palstra T T M, Lu G, Menovsky A A, Nieuwenhuys G J, Kes P H and Mydosh J A 1986 *Phys. Rev.* B **34** 4566